Structure of the Regulatory Domain of Human Cardiac Troponin C in Complex with the Switch Region of Cardiac Troponin I and the Drug W7: The Basis of W7 as an Inhibitor of Cardiac M...

ARTICLE *in* JOURNAL OF MOLECULAR AND CELLULAR CARDIOLOGY · MAY 2010

Impact Factor: 4.66 · DOI: 10.1016/j.yjmcc.2010.01.016 · Source: PubMed

4 AUTHORS, INCLUDING:

Marta Oleszczuk
University of Alberta
30 PUBLICATIONS **321** CITATIONS
SEE PROFILE

Ian Robertson
Government of Alberta
25 PUBLICATIONS **173** CITATIONS
SEE PROFILE

Monica X Li
University of Alberta
51 PUBLICATIONS **2,141** CITATIONS
SEE PROFILE

Journal of Molecular and Cellular Cardiology 48 (2010) 925–933

Contents lists available at ScienceDirect

Journal of Molecular and Cellular Cardiology

journal homepage: www.elsevier.com/locate/yjmcc

Original article

Solution structure of the regulatory domain of human cardiac troponin C in complex with the switch region of cardiac troponin I and W7: The basis of W7 as an inhibitor of cardiac muscle contraction

Marta Oleszczuk, Ian M. Robertson, Monica X. Li, Brian D. Sykes *

Department of Biochemistry, School of Molecular and Systems Medicine, University of Alberta, Edmonton, Alberta, Canada T6G 2H7

ARTICLE INFO

Article history:
Received 21 December 2009
Received in revised form 19 January 2010
Accepted 20 January 2010
Available online 29 January 2010

Keywords:
Troponin
Structure
Drugs
Mechanism
Inhibition

ABSTRACT

The solution structure of Ca^{2+}-bound regulatory domain of cardiac troponin C (cNTnC) in complex with the switch region of troponin I ($cTnI_{147–163}$) and the calmodulin antagonist, *N*-(6-aminohexyl)-5-chloro-1-naphthalenesulfinamide (W7), has been determined by NMR spectroscopy. The structure reveals that the W7 naphthalene ring interacts with the terminal methyl groups of M47, M60, and M81 as well as aliphatic and aromatic side chains of several other residues in the hydrophobic pocket of cNTnC. The H3 ring proton of W7 also contacts the methyl groups of I148 and M153 of $cTnI_{147–163}$. The *N*-(6-aminohexyl) tail interacts primarily with the methyl groups of V64 and M81, which are located on the C- and D-helices of cNTnC. Compared to the structure of the cNTnC•Ca^{2+}•W7 complex (Hoffman, R. M. B. and Sykes, B. D. (2009) *Biochemistry* 48, 5541–5552), the tail of W7 reorients slightly toward the surface of cNTnC while the ring remains in the hydrophobic pocket. The positively charged $–NH_3^+$ group from the tail of W7 repels the positively charged R147 of $cTnI_{147–163}$. As a result, the N-terminus of the peptide moves away from cNTnC and the helical content of $cTnI_{147–163}$ is diminished, when compared to the structure of cNTnC•Ca^{2+}•$cTnI_{147–163}$ (Li, M. X., Spyracopoulos, L., and Sykes B. D. (1999) *Biochemistry* 38, 8289–8298). Thus the ternary structure cNTnC•Ca^{2+}•W7•$cTnI_{147–163}$ reported in this study offers an explanation for the ~13-fold affinity reduction of $cTnI_{147–163}$ for cNTnC•Ca^{2+} in the presence of W7 and provides a structural basis for the inhibitory effect of W7 in cardiac muscle contraction. This generates molecular insight into structural features that are useful for the design of cTnC-specific Ca^{2+}-desensitizing drugs.

A healthy human heart generates ~3 billion contractile cycles over an average life span. Each contractile cycle involves systolic activation and diastolic relaxation, regulated by Ca^{2+} association and dissociation from troponin in the cardiac myofilaments. Troponin is a heterotrimeric complex composed of the Ca^{2+}-binding subunit, troponin C (cTnC), inhibitory subunit, troponin I (cTnI), and the tropomyosin-binding subunit, troponin T (cTnT). During diastole, troponin holds tropomyosin in a conformational state that blocks the interaction between myosin and actin. When Ca^{2+} binds cTnC during systole, the switch region of cTnI associates with the N-domain of cTnC (cNTnC). This is coupled with the removal of the inhibitory region of cTnI from actin so that the troponin–tropomyosin complex no longer inhibits the actin–myosin interaction. Subsequently, tension producing actin–myosin cross bridges form, which potentiates actomyosin ATPase activity, and ultimately force generation (for reviews, see [1,2]).

In diseased heart, the contractile cycle is compromised by either Ca^{2+} desensitization with diminished systolic contractility (e.g., in cases of congestive heart failure) or Ca^{2+} oversensitization accompanied with insufficient diastolic relaxation (e.g., in cases of hypertrophic cardiomyopathy). The ability to sensitize or desensitize cardiac muscle to Ca^{2+} has therapeutic potential for the treatment of cardiac dysfunction. Ideally, this mechanism would avoid altering Ca^{2+} transients in myocardial cells, which would perturb the regulation of other Ca^{2+}-based signaling pathways, but rather involve modulating the altered Ca^{2+} response of the myofilaments (for a review, see [3]). The essential role of troponin in the regulation of the contractile cycle makes it an attractive and logical target for the design of cardiotonic drugs. Toward this goal, a group of Ca^{2+}-sensitizing drugs have been developed. One example is levosimendan, a novel Ca^{2+} sensitizer discovered by using cTnC as a target protein (for a recent review, see [4]). This drug has been proved to be a well-tolerated, effective treatment for patients with severe decompensated heart failure. A recent study has shown that a myosin inhibitor, blebbistatin (1-phenyl-1,2,3,4-tetrahydro-4-hydroxypyrrolo(2,3-b)-7-methylquinolin-4-one), functions as an effective Ca^{2+} desensitizer in cardiac

Abbreviations: TnC, troponin C; cTnC, cardiac troponin C; cNTnC, N-domain (residues 1–89) of cTnC; cCTnC, C-domain (residues 91–161) of cTnC; sTnC, skeletal troponin C; CaM, calmodulin; TnI, troponin I; cTnI, cardiac troponin I; $cTnI_{147–163}$, cTnI peptide acetyl-RISADAMMQALLGARAK-amide; sTnI, skeletal troponin I; $sTnI_{115–131}$, sTnI residues 115–131; TFP, trifluoperazine.

* Corresponding author. Tel.: +1 780 492 5460; fax: +1 780 492 0886.
E-mail address: brian.sykes@ualberta.ca (B.D. Sykes).

0022-2828/$ – see front matter © 2010 Elsevier Ltd. All rights reserved.
doi:10.1016/j.yjmcc.2010.01.016

muscle contraction without causing arrhythmia, suggesting that Ca^{2+} desensitization might be beneficial to individuals with hypertrophic cardiomyopathy [5].

Many hydrophobic compounds are known to bind to CaM and perturb CaM–target interactions. Because of the structural homology between cTnC and CaM, these agents may also interact with cTnC and be good candidates as cardiotonic drugs. An earlier study has shown that some CaM antagonists (calmidazolium, bepridil, trifluoperazine, chlorpromazine, pimozide) stimulate myofibrillar ATPase activity while others (W7, haloperiodol, mastoparan) inhibit ATPase activity [6]. This suggests that CaM antagonists differentially affect the properties of troponin, probably via different modes of action on the cTnC–cTnI interface. Structural studies have identified multiple binding sites of TFP and bepridil on cTnC [7]. In the X-ray structure of the cTnC•3Ca^{2+}•3bepridil complex [8], two bepridil molecules pull the N- and C-domains close together to result in a compact structure for cTnC, while a third bepridil appears to stabilize an open regulatory domain conformation by binding to the hydrophobic pocket much like the switch region of cTnI ($cTnI_{147–163}$) as shown in the structures of cNTnC•Ca^{2+}•$cTnI_{147–163}$ [9] and cTnC•3Ca^{2+}•$cTnI_{31–210}$•$cTnT_{183–288}$ [10] complexes. The NMR structure of the cNTnC•Ca^{2+}•$cTnI_{147–163}$•bepridil complex shows that bepridil and $cTnI_{147–163}$ bind to the hydrophobic pocket of cNTnC•Ca^{2+} concurrently [11]. In the X-ray structure of cNTnC•Ca^{2+}•2TFP (PDB: 1WRK and 1WRL), two TFP molecules fit in the hydrophobic pocket of cNTnC•Ca^{2+} with the $–CF_3$ group of each TFP pointed toward the hydrophobic cleft. When compared to the structure of cNTnC•Ca^{2+}•$cTnI_{147–163}$•bepridil, it appears that one of the TFP molecules would be replaced by $cTnI_{147–163}$ peptide. In the X-ray structure of the sTnC•4Ca^{2+}•$sTnI_{1–182}$•$sTnT_{156–262}$ complex [12], a polyoxyethylene detergent molecule, anapoe, binds specifically to the Ca^{2+}-saturated N-domain of sTnC together with the switch region of sTnI ($sTnI_{115–131}$) and this binding is likely responsible for the increase of the contractile force of muscle fibers in the presence of anapoe. The Ca^{2+}-sensitizing effect of levosimendan has been shown to be due to a network of interactions between the drug, cNTnC, and $cTnI_{144–163}$ (a longer version of switch region of cTnI) that creates a binding site for levosimendan and the net result is the stabilization of the open conformation of cNTnC•Ca^{2+}[13].

W7 is a CaM antagonist that has been used to explore a wide range of physiological processes involving Ca^{2+} signaling in cardiomyocytes. Focusing on delineating the role of W7 in the interplay of troponin- and myosin-based pathways of Ca^{2+} activation in skeletal and cardiac muscle, Adhikari and Wang have shown that in both skeletal and cardiac muscle fibers, W7 inhibits the maximum ATPase activity and Ca^{2+} sensitivity [14]. The W7 inhibition is most likely mediated via specific interactions between W7 and TnC. This notion is supported by the observation that W7 binds specifically to TnC and not to tropomyosin, actin, or myosin [15]. We have shown that W7 binds specifically to cNTnC, and this binding can occur concurrently with the switch region of cTnI [16]. Moreover, we have shown that the affinity of W7 for cNTnC in the cTnC•3Ca^{2+}•$cTnI_{34–71}$•$cTnI_{128–163}$ complex is ~2-fold weaker than for the isolated cNTnC•Ca^{2+}[17]. This is in line with the functional data demonstrating that W7 is an effective inhibitor in cardiac muscle contraction. We have also determined the solution structure of cNTnC•Ca^{2+}•W7 that located the binding site of W7 in the hydrophobic pocket of cNTnC•Ca^{2+}[18].

In order to elucidate the mechanism of W7 inhibition, we have determined the solution structure of a ternary cNTnC•Ca^{2+}•$cTnI_{147–163}$•W7 complex. In the structure, $cTnI_{147–163}$ binds at the A/B interhelical interface and W7 binds in the hydrophobic cavity formed between cNTnC•Ca^{2+} and $cTnI_{147–163}$. In the structure, the N-terminal R147 of $cTnI_{147–163}$ is electrostatically repelled from the positively charged tail of the W7, and thus moves away from cNTnC•Ca^{2+}. This offers an explanation for the ~13-fold affinity reduction of $cTnI_{147–163}$ for cNTnC•Ca^{2+} in the presence of W7. The structure provides insights into the design of cardiotonic drugs that modulate the Ca^{2+} sensitivity of the myofilament via perturbation of the cTnC–cTnI interaction.

1. Materials and methods

1.1. Sample preparation

The engineering of the cNTnC (1–89) construct and the expression of ^{15}N- and $^{15}N/^{13}C$-labeled cNTnC in *E. coli* were as described previously [11]. The synthetic peptide $cTnI_{147–163}$, acetyl-RISADAMM-QALLGARAK-amide, was obtained from GL Biochem (Shanghai, China). The purity and mass were verified by HPLC and electrospray mass spectrometry, respectively. W7 was purchased from Sigma-Aldrich. Stock solutions of 100 mM W7 in DMSO-d_6 (Cambridge Isotopes) were prepared and since W7 is sensitive to light, the vial was wrapped in aluminum foil. All NMR samples were 500 µl in volume. The buffer conditions were 100 mM KCl, 10 mM imidazole in 90% H_2O/10% D_2O or 5% H_2O/95% D_2O, 15 mM dithiothreitol (DTT), 0.5 mM 3-(trimethylsilyl)-1-propanesulfonic acid (DSS), and the pH adjusted to 6.8. For structure determination, NMR samples contain 0.7 mM cNTnC, 7 mM Ca^{2+}, 3 mM W7, and 3.2 mM $cTnI_{147–163}$.

1.2. $cTnI_{147–163}$ titration of ^{15}N-cNTnC•Ca^{2+}•W7

Previously, $cTnI_{147–163}$ was titrated into ^{15}N-cNTnC•Ca^{2+} in the absence of W7 [9]. The titration was performed by adding solid peptide and amino acid analysis was used to determine the peptide/protein ratio at every titration point. This is because $cTnI_{147–163}$ peptide is only soluble in aqueous solution at low concentrations (~1 mM) and tends to form a gel at higher concentrations. A similar procedure was employed in this work for the titration of $cTnI_{147–163}$ to ^{15}N-cNTnC•Ca^{2+} in the presence of W7. The sample was mixed thoroughly with each addition. Changes in pH associated with $cTnI_{147–163}$ additions were compensated by adjusting to pH 6.8 at every titration point. 1D ^1H and 2D ^1H,^{15}N-HSQC NMR spectra of ^{15}N-cNTnC were acquired at every titration point.

1.3. NMR spectroscopy

NMR data used in this study were collected at 30 °C using Varian Inova 800-MHz, Unity 600-MHz, and Varian Inova 500-MHz spectrometers. All spectrometers are equipped with triple resonance probes with Z-pulsed field gradients. The chemical shifts of backbone and side chain atoms of cNTnC as well as the bound W7 and $cTnI_{147–163}$ were assigned using 2D and 3D NMR experiments outlined in the Supplemental Table S1. 1D ^1H and 2D DQF-COSY spectra of free W7 in DMSO-d_6 were obtained (as described in Hoffman and Sykes [18]) to help in the assignment of the W7 in the ternary complex. 2D DQF-COSY NMR spectra of an NMR sample of cNTnC•Ca^{2+}•$cTnI_{147–163}$•W7 in D_2O were acquired for the assignment of bound W7. Resonances for aromatic residues were assigned using 2D homonuclear DQF-COSY and NOESY experiments in D_2O. 2D $^{13}C/^{15}N$-filtered TOCSY and 2D $^{13}C/^{15}N$-filtered NOESY [19-21] spectra of a sample of cNTnC•Ca^{2+}•$cTnI_{147–163}$•W7 in H_2O were acquired for the assignment of bound W7 and bound $cTnI_{147–163}$. The intermolecular NOEs between W7 and $cTnI_{147–163}$ were assigned from 2D $^{13}C/^{15}N$-filtered NOESY. The intermolecular NOEs between $^{13}C/^{15}N$-labeled cNTnC and unlabeled $cTnI_{147–163}$ and W7 were obtained using 3D-^{13}C-edited HMQC-NOESY [22,23] experiment with 150-ms mixing time.

1.4. Data processing and peak calibration

All 2D and 3D NMR data were processed using NMRPipe [24] and all 1D NMR data were processed using VNMRJ (Varian). Assignment of chemical shifts was carried out in NMRViewJ [25]and backbone

Table 1
Structural statistics of the family of the 20 structures calculated.

Intramolecular NOE restraints in cNTnC		
Total	1184 (~13/residue)	
Short range ($\|i•j\| \leq 1$)	817	
Medium range ($2 \leq \|i•j\| \leq 4$)	211	
Long range ($\|i•j\| \geq 5$)	156	
Dihedral restraints in cNTnC		
ϕ	59	
ψ	57	
Intermolecular NOEs between cNTnC and W7	30	
Intermolecular NOEs between cNTnC and the $cTnI_{147-163}$ peptide	24	
Intermolecular NOEs between the $cTnI_{147-163}$ peptide and W7	3	
Intramolecular NOE restraints in W7	6	
Intramolecular restraints in $cTnI_{147-163}$ peptide		
NOEs	15	
ϕ angle restraints	5	
ψ angle restraints	5	
Artificial restraints to Ca^{2+}	6	
NOE violations/structure>0.2 Å		
Before water refinement	0.0 ± 0.0	
After water refinement	8.7 ± 2.1	
Dihedral violations/structure>1°		
Before water refinement	0.55 ± 0.12	
After water refinement	1.00 ± 0.22	
ϕ, ψ in core or allowed regions[a]		
Before water refinement	99.5%	
After water refinement	98.9%	
RMSD from the average structure (Å)[b]		
	Well-defined residues	Helices
Before water refinement	0.80 ± 0.11	0.32 ± 0.05
After water refinement	0.87 ± 0.12	0.37 ± 0.06

[a] As determined using PROCHECK.
[b] Well-defined backbone atoms (N, C, CA) with RMSD smaller than 1Å. The RMSD. for helices are calculated from the weighted mean average of the RMSD of individual helices.

assignments were aided with the software package SmartNotebook [26]. The chemical shifts that were assigned in NMRView were converted to CYANA nomenclature, for NOE calibration. Initial structures of cNTnC were generated using program CYANA 2.1. Unambiguous restraints were assigned manually and were forced to keep their assignments during the first four runs of CYANA[27] calculations, after which they were open for automatic assignment with the "noeassign" script of CYANA. Distance restraints were calibrated with CYANA standard procedure using upper limits of 6 Å. After the CYANA refinement, the final restraints were converted to XPLOR-NIH [28,29] nomenclature. Intramolecular NOEs of $cNTnI_{147-163}$ and W7 and all intermolecular NOEs were assigned manually and categorized as weak (1.8–6.0 Å).

1.5. Coordinates and topology of W7

Representation of W7 was defined using HIC-Up and XPLO2D servers (http://xray.bmc.uu.se) and checked manually. Positive charge on W7 tail ($-CH_2-NH_3^+$ group) was added manually in analogy to positive charge on $-CH_2-NH_3^+$ group in LYS+.

1.6. Structural calculations

Dihedral angle restraints from TALOS [30,31] as well as 6 distance restraints from X-ray crystallographic data of chelating oxygen atoms to the Ca^{2+} ion in site II were used for structure calculation in addition to NOE distance restraints. The 20 conformers of cNTnC obtained from CYANA were averaged in XPLOR-NIH and used as a template structure in the simulated annealing protocol, with 10,000 high-temperature steps and 6000 cooling steps. After the structure of cNTnC was well defined, the ternary cNTnC•Ca^{2+}•$cTnI_{147-163}$•W7 structure was solved in a similar manner, starting with an extended conformation of cNTnC. The intramolecular and intermolecular NOE restraints used in the calculations are summarized in Table 1. Thirty lowest energy conformers of the 300 calculated were refined in explicit solvent by XPLOR-NIH with a water box edge length of 18.8 Å. The final ensemble discussed in this article represents the 20 lowest energy conformers obtained after water refinement (see Table 1 for statistics). The final refined ensemble has been deposited in the protein data bank (www.rcsb.org) with the PDB accession code of 2KRD.

2. Results and discussion

2.1. Effect of W7 on the stability of cNTnC•Ca^{2+}•$cTnI_{147-163}$

We have previously characterized the interaction of $cTnI_{147-163}$ and cNTnC•Ca^{2+} and determined the affinity of $cTnI_{147-163}$ for cNTnC•Ca^{2+} ($K_D = 154 \pm 30$ μM) [9]. In the present study, the assigned 2D ^1H, ^{15}N-

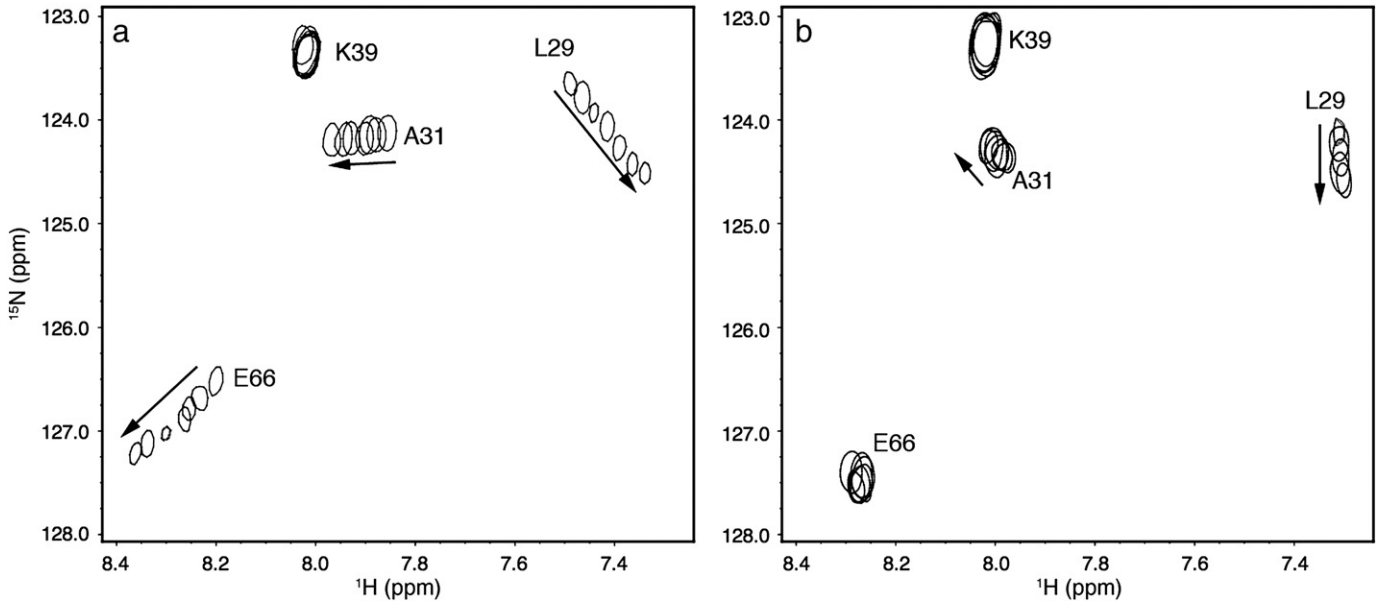

Fig. 1. Titration of (a) cNTnC•$Ca^{2+}$and (b) cNTnC•Ca^{2+}•W7, respectively, with $cTnI_{147-163}$. 2D ^1H, ^{15}N-HSQC NMR spectra for residues L29, A31, K39, and E66 of cNTnC at various peptide additions are superimposed, showing the progressive shift of peaks with increasing $cTnI_{147-163}$ concentrations.

HSQC NMR spectrum of cNTnC•Ca^{2+}•W7 was used to monitor the binding of $cTnI_{147-163}$ to cNTnC•Ca^{2+}•W7. Using four residues (L29, A31, K39, and E66) as examples, a comparison of the $cTnI_{147-163}$-induced 2D ^{1}H, ^{15}N-HSQC NMR peak shifts of cNTnC•Ca^{2+} and of cNTnC•Ca^{2+}•W7 is depicted in Figs. 1a and b, respectively. In both titrations, the chemical shift changes fall into the fast exchange limit on the NMR scale, and the movement of the cross peaks indicates that the binding of $cTnI_{147-163}$ to cNTnC•Ca^{2+} or cNTnC•Ca^{2+}•W7 occurs with a 1:1 stoichiometry (Supplemental Fig. S1). The $cTnI_{147-163}$-induced chemical shift changes are larger in Fig. 1a, corresponding to a closed to open conformational transition in cNTnC as characterized previously [9]. The smaller $cTnI_{147-163}$-induced chemical shift changes in Fig. 1b corresponds to the binding of $cTnI_{147-163}$ to an already partially open cNTnC in the cNTnC•Ca^{2+}•W7 complex [18]. Plotting the chemical shift changes in Fig. 1b as a function of the peptide to protein ratio, a binding dissociation constant (K_D) of 2000 ± 50 μM gives the best fit as shown in Supplemental Fig. S1. A global fitting for the titration of $cTnI_{147-163}$ to cNTnC•Ca^{2+} is also shown in Supplemental Fig. S1 for the purpose of a direct comparison. This suggests that the affinity of $cTnI_{147-163}$ for cNTnC•Ca^{2+} is decreased ~13-fold (from 154 ± 30 μM to 2000 ± 50 μM) by the presence of W7. This helps explain why W7 is effective in inhibiting the activity of actomyosin ATPase and force generation in muscle fibers [6,14].

2.2. Overall structure of the ternary complex

The 2D ^{1}H, ^{15}N-HSQC NMR spectrum of cNTnC in the ternary cNTnC•Ca^{2+}•$cTnI_{147-163}$•W7 complex is well resolved, allowing the chemical shifts of the backbone and the side chain atoms to be assigned using ^{15}N- and/or $^{15}N/^{13}C$-labeled protein. Intramolecular distance restraints for cNTnC in the ternary complex were obtained by analyzing the 3D ^{15}N- and ^{13}C-edited NOESY experiments. Dihedral angle restraints for cNTnC in the ternary complex were obtained from TALOS [30,31].

The proton NMR chemical shift assignments and intramolecular distance restraints for the bound $cTnI_{147-163}$ and W7 required the collection of $^{15}N/^{13}C$-filtered 2D-TOCSY and 2D-NOESY experiments using unlabeled $cTnI_{147-163}$ and W7 in complex with $^{15}N/^{13}C$-labeled cNTnC. These experiments removed all of the resonance peaks arising from $^{15}N/^{13}C$-labeled cNTnC. 2D DQF-COSY NMR spectra of free (see

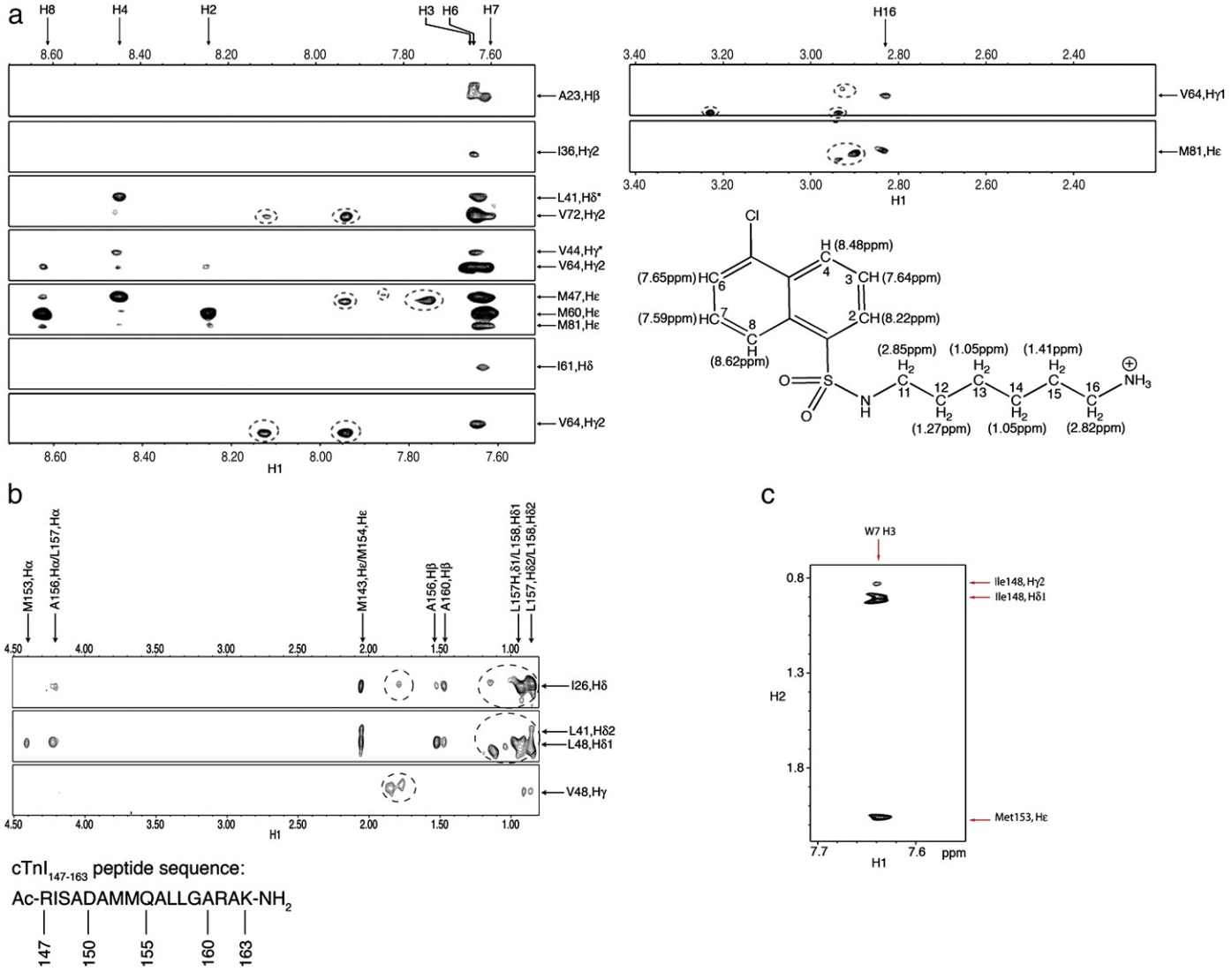

Fig. 2. Intermolecular NOE contacts (a) between cNTnC•Ca^{2+} and W7, (b) between cNTnC•Ca^{2+} and $cTnI_{147-163}$, and (c) between $cTnI_{147-163}$ and W7. The NMR sample of cNTnC•Ca^{2+}•$cTnI_{147-163}$•W7 contains 0.7 mM cNTnC, 7 mM Ca^{2+}, 3.4 mM $cTnI_{147-163}$, and 3 mM W7. (a) The chemical structure of W7. The number designation and the chemical shift assignments of W7 are indicated. Strips from the 3D $^{15}N/^{13}C$-edited HMQC-NOESY NMR experiments showing the intermolecular NOE contacts between the ring of W7 and cNTnC and between the tail of W7 and cNTnC. The circled peaks are intermolecular NOE contacts between the $cTnI_{147-163}$ peptide and cNTnC (left panel) and are unassigned (right panel). (c) The sequence of $cTnI_{147-163}$ peptide. Sample strips from the 3D $^{15}N/^{13}C$-edited HMQC-NOESY NMR experiments showing the intermolecular NOE contacts between cNTnC and $cTnI_{147-163}$. (c) Intermolecular NOE contacts between the methyl groups of I148 and M153 of $cTnI_{147-163}$ to H3 from the naphthalene ring of W7, obtained from 2D $^{15}N/^{13}C$-filtered-NOESY NMR spectra.

[18]) and bound W7 (see Supplemental Fig. S2) were also acquired to aid in the assignment of bound W7. Intermolecular NOEs between cNTnC and W7 (Fig. 2a) and between cNTnC and $cTnI_{147–163}$ (Fig. 2b) were determined from 3D ^{13}C-edited/filtered HMQC-NOESY data. These experiments were optimized for detecting NOEs between protons attached to ^{12}C and protons attached to aliphatic ^{13}C, thereby editing out all the intramolecular NOEs. Three intermolecular NOEs between $cTnI_{147–163}$ and W7 were obtained from the $^{15}N/^{13}C$-filtered 2D NOESY experiment (Fig. 2c). A total of 1264 NOE distance restraints was used for structure calculations. These include 1184 intramolecular cNTnC distance restraints (~13 restraints per residue), 15 intramolecular $cTnI_{147–163}$ distance restraints, 6 intramolecular W7 distance restraints, 24 intermolecular contacts between cNTnC and $cTnI_{147–163}$, 30 intermolecular contacts between cNTnC and W7, and 3 intermolecular contacts between $cTnI_{147–163}$ and W7; 116 dihedral restraints for cNTnC, 10 dihedral restraints for $cTnI_{147–163}$, and 6 artificial distance restraints to Ca^{2+} were used to calculate the structure of the cNTnC•Ca^{2+}•$cTnI_{147–163}$•W7 complex (see Table 1). Fig. 3a depicts the ensemble of the 20 lowest energy structures of the ternary complex in stereo view, with overall structural statistics and conformational energies for the ensemble provided in Table 1. The ribbon representations of the structure of the ternary complex are shown in Fig. 3b. The structure of cNTnC in the complex is better defined than those of $cTnI_{147–163}$ or W7, as a result of more restraints for the protein than for the ligands.

2.3. Structure of cNTnC in the ternary complex

cNTnC in the present structure exhibits an overall fold resembling other Ca^{2+}-bound domains in the EF-hand family. The secondary structural elements of cNTnC in the ternary cNTnC•Ca^{2+}•$cTnI_{147–163}$•W7 complex are similar to those in the cNTnC•apo (PDB: 1SPY), cNTnC•Ca^{2+} ((PDB: 1AP4), cNTnC•Ca^{2+}•W7 (PDB: 2KFX), cNTnC•Ca^{2+} •$cTnI_{147–163}$ (PDB: 1MXL), and cNTnC•Ca^{2+}•$cTnI_{147–163}$•bepridil (PDB: 1LXF) complexes. The five helices, N, A, B, C, and D, are well defined, superimposing with individual backbone RMSDs of 0.31 ± 0.12 Å for helix N (residues 5–11), 0.54 ± 0.14 Å for helix A (residues 14–27), 0.20 ± 0.13 Å for helix B (residues 41–46), 0.39 ± 0.13 Å for helix C (residues 54–63), and 0.42 ± 0.11 Å for helix D (residues 74–86). The two EF-hand Ca^{2+}-binding sites are joined by a short anti-parallel β-sheet. The β-sheet (residues 35–37, 71–73) is well defined with a backbone RMSD of 0.39 ± 0.09 Å, while the Ca^{2+}-binding sites have a slightly more flexible structure (a backbone RMSD of 0.92 ± 0.28 Å). The N- and C-terminal residues (residues 1–4 and 86–89) are less well defined than the helices or the β-sheet. The global fold and the orientations of the five helices of cNTnC in the ternary cNTnC•Ca^{2+} •$cTnI_{147–163}$•W7 complex are similar to the open cNTnC•Ca^{2+}•$cTnI_{147–163}$, cNTnC•Ca^{2+}•W7, and cNTnC•Ca^{2+}•$cTnI_{147–163}$•bepridil structures (see Fig. 5). The effects of $cTnI_{147–163}$ and W7 on the structural fold of cNTnC will be discussed below.

2.4. Structure of W7 in the ternary complex

W7 consists of a naphthalene group and an *N*-(6-aminohexyl) tail (Fig. 2a). The binding site and conformation of W7 in the ternary complex is similar as in the structure of cNTnC•Ca^{2+}•W7. The orientation of W7 was determined by intermolecular NOEs between cNTnC and W7 and between $cTnI_{147–163}$ and W7. Strip plots taken from the 3D $^{15}N/^{13}C$ F_1-filtered, F_3-edited spectra of cNTnC•Ca^{2+} •$cTnI_{147–163}$•W7 complex are shown in Figs. 2a and b. In the spectra,

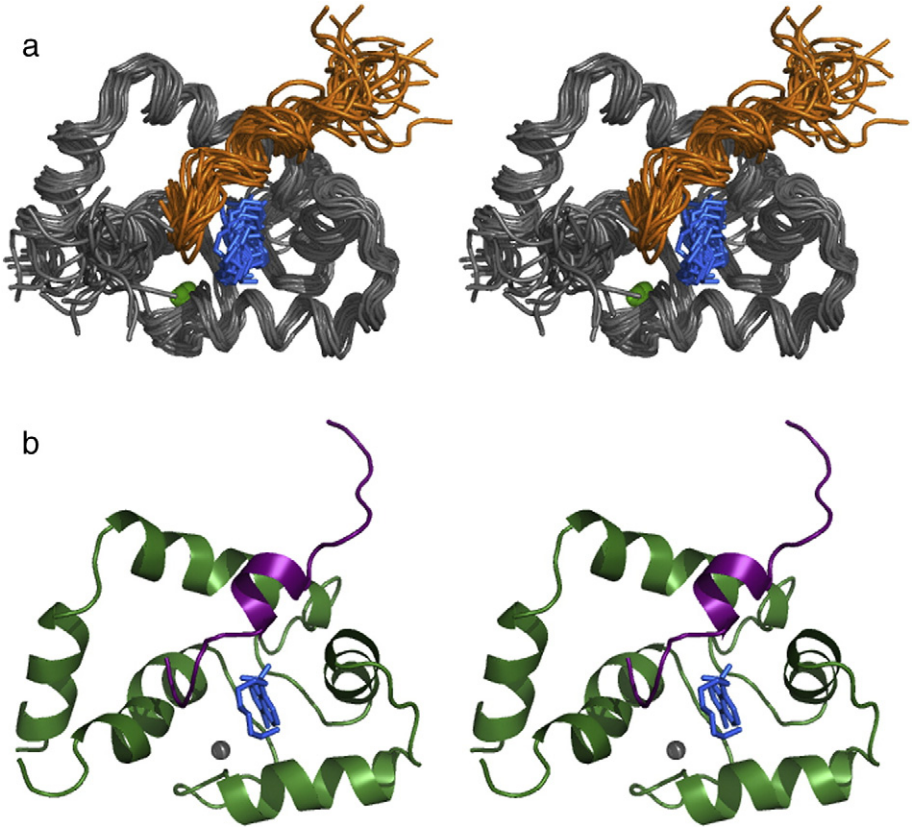

Fig. 3. (a) The solution structure of the cNTnC•Ca^{2+}•$cTnI_{147–163}$•W7 complex in stereo view. The backbones (N, Cα, C') of a family of 20 structures are shown in gray. The assembly of the $cTnI_{147–163}$ structures is shown in gold. The assembly of W7 is shown in blue. The Ca^{2+} ions are shown as green spheres. (b) The ribbon representation of the lowest energy structure in stereo view. The protein is shown in green and Ca^{2+} ions are shown as gray spheres. Heavy atom skeleton of W7 is shown in blue. The $cTnI_{147–163}$ peptide is shown in purple.

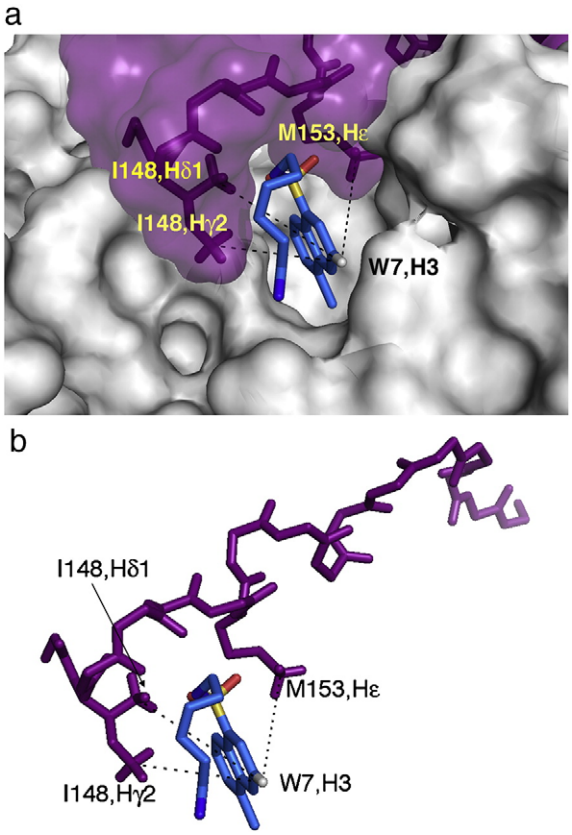

Fig. 4. A close-up view of the skeleton representation of the peptide backbone and W7, showing the interaction between $cTnI_{147-163}$ and W7 (a) with and (b) without the protein surface present.

only NOEs arising from the ^{12}C-attached protons in $cTnI_{147-163}$ and W7 and terminating on ^{13}C-attached protons in cNTnC are observed. The naphthalene ring of W7 makes a number of contacts with residues that line the hydrophobic pocket of cNTnC, such as A23, L41, V44, M47, M60, I61, M81, I36, V64, and V72. As a result, the naphthalene ring of W7 is nestled deep in the hydrophobic cleft. The contacts between H3 of W7 and the methyl groups of I148 and M153 of $cTnI_{147-163}$ fix the orientation of the bicyclic ring relative to $cTnI_{147-163}$ (Fig. 4). The *N*-(6-aminohexyl) tail of W7 makes contacts to the C/D helices of cNTnC (e.g., H16 to the methyl groups of V64 and M81). The positively charged $-NH3^+$ moiety of W7 and the N-terminal R147 of $cTnI_{147-163}$ repel each other and the two ligands reorient their positions relative to those in the binary cNTnC•Ca^{2+}•$cTnI_{147-163}$ or the cNTnC•Ca^{2+}•W7 complex to accommodate each other in the hydrophobic pocket of cNTnC•Ca^{2+} (see below). When the heavy atoms of W7 superimpose onto the average structure in the ternary complex, the average RMSD for the naphthalene group is 1.1 Å, while that for the tail is 2.1 Å.

2.5. Structure of $cTnI_{147-163}$ in the ternary complex

The structure of $cTnI_{147-163}$ when complexed with cNTnC•Ca^{2+} has been determined in three separate structures. In the structure of cNTnC•Ca^{2+}•$cTnI_{147-163}$, residues 150–157 form a short α-helix. This short helix was defined primarily by the use of chemical shift index and several intermolecular NOE restraints between cNTnC and the peptide (there were no intramolecular NOEs assigned). In the structure of cNTnC•Ca^{2+}•$cTnI_{147-163}$•bepridil, 24 intramolecular NOEs including 3 d_{NN} and 6 $d_{\alpha N}(i,i+3)$ (the hallmark of a helical structure) restraints for the 17-residue $cTnI_{147-163}$ peptide were assigned. A combination of these NOEs and the dihedral angle restraints better defined the peptide. In the X-ray structure of the core domain cardiac troponin, cTnC•3Ca^{2+}•$cTnI_{34-210}$•$cTnT_{182-288}$, this fragment of cTnI displays a

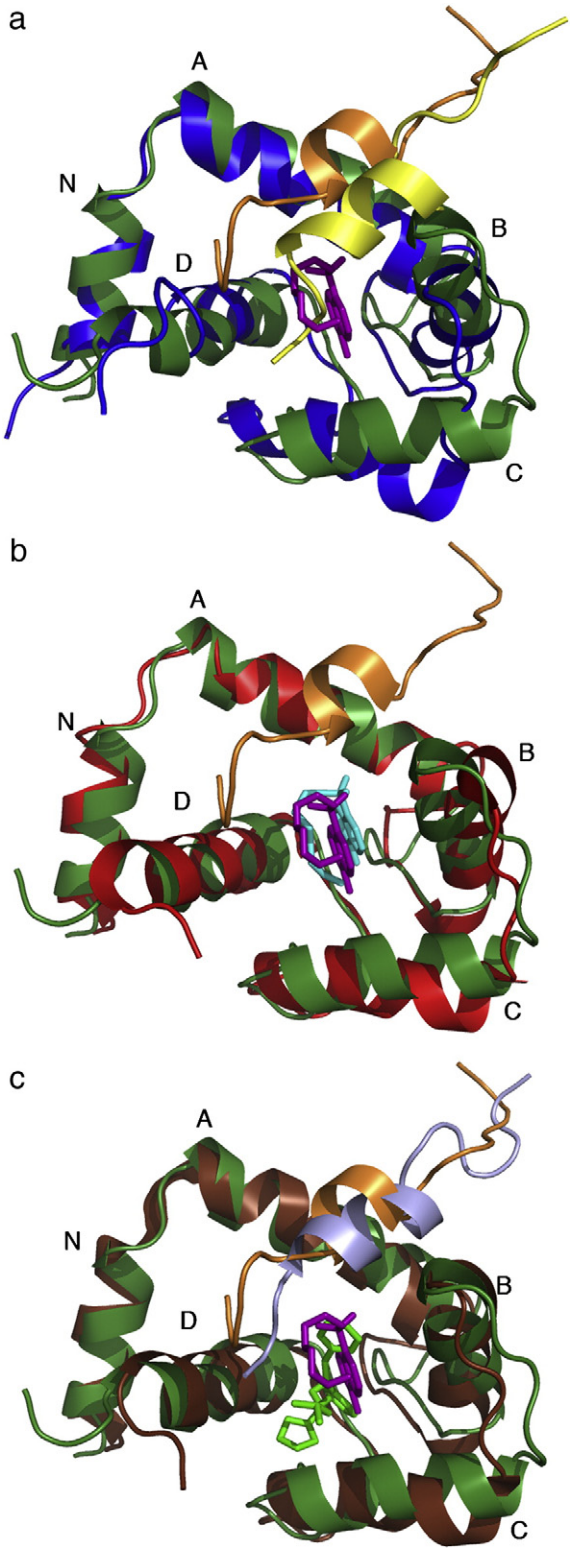

Fig. 5. (a) Backbone overlay of cNTnC in the cNTnC•Ca^{2+}•$cTnI_{147-163}$•W7 complex (dark green) and cNTnC in the cNTnC•Ca^{2+}•$cTnI_{147-163}$ complex (blue). Note the position shift and helical content changes of $cTnI_{147-163}$ from yellow to gold in the presence of W7 (purple). (b) Backbone overlay of cNTnC in the cNTnC•Ca^{2+}•$cTnI_{147-163}$•W7 complex (dark green) and cNTnC in the cNTnC•Ca^{2+}•W7 complex (red). Note the change of position of W7 from cyan to purple when $cTnI_{147-163}$ is present. (c) Backbone overlay of cNTnC in the cNTnC•Ca^{2+}•$cTnI_{147-163}$•W7 complex (cNTnC in dark green, $cTnI_{147-163}$ in gold, W7 in purple) and cNTnC in the cNTnC•Ca^{2+}•$cTnI_{147-163}$•bepridil complex (cNTnC in brown, $cTnI_{147-163}$ in lavender, bepridil in light green).

Table 2
Interhelical angles of various EF hands.

Calcium binding protein	Interhelical angles(°)[a]		Accession code (PDB)
	A/B	C/D	
cNTnC·apo (NMR)	140±3	128±4	1SPY
cNTnC·Ca^{2+} (NMR)	132±3	113±4	1AP4
cNTnC·Ca^{2+}·$cTnI_{147-163}$ (NMR)	102±5	96±5	1MXL
cTnC·3Ca^{2+}·$cTnI_{31-210}$·$cTnT_{183-288}$ (X-ray)	103	96	1J1E
cNTnC·Ca^{2+}·bepridil·$cTnI_{147-163}$ (NMR)	121±4	91±4	1LXF
cTnC·3Ca^{2+}·bepridil (X-ray)	92	90	1DTL
cNTnC·Ca^{2+}·W7 (NMR)	114±3	92±2	2KFX
cNTnC·Ca^{2+}·W7·$cTnI_{147-163}$ (NMR)	113±5	66±4	2KRD
CaM(N-domain)·Ca^{2+}·W7 (NMR)	102±4	75±5	1MUX
CaM(C-domain)·Ca^{2+}·W7 (NMR)	105±4	85±4	1MUX

The axis for an α-helix is defined by two points, taken as the average coordinates of the first and last 11 backbone atoms of the α-helix. Interhelical angles were calculated using the program interhelix (K. Yap, University of Toronto).

[a] The 180° interhelical angle corresponds to a completely closed EF-hand domain (anti-parallel helices), whereas 0° angle defines a completely open conformation (parallel helices). The extent of openness is characterized by the A/B and C/D interhelical angles. cNTnC in 2KRD is open as compared to the closed 1SPY or 1AP4. The A/B helical pair is more closed than 1MXL, while the C/D pair is more open. As compared to 2KFX, the A/B pair is similar but the C/D pair is more open. Both the A/B and C/D pairs of 2KRD are more open than cNTnC in 1LXF. While the C/D helical pair in this complex is more open than that in all the open cNTnC structures, it is similar to the corresponding helical pair in CaM(N-domain)•2Ca^{2+}•W7 and CaM(C-domain)•2Ca^{2+}•W7.

near identical structure as in the two NMR structures (superimpose to 0.2 Å). In the present structure, cNTnC•Ca^{2+}•$cTnI_{147-163}$•W7, the $cTnI_{147-163}$ conformation is calculated by using both intra- and intermolecular NOEs and dihedral restraints. The overall conformation and orientation is similar to those in the other three structures but the helical component is diminished. In the ensemble of solution structures (Fig. 3), the backbone atoms of the 17 residues superimpose on to the average peptide structure with an RMSD of 1.9±0.3 Å. The assigned intermolecular NOEs are summarized in Fig. 2. These NOE contacts dictate a similar orientation for the $cTnI_{147-163}$ in the ternary cNTnC•Ca^{2+}•$cTnI_{147-163}$•W7 complex as compared to that in the cNTnC•Ca^{2+}•$cTnI_{147-163}$ or cNTnC•Ca^{2+}•$cTnI_{147-163}$•bepridil complexes. The peptide inserts between the A/B helices in cNTnC with the N-terminus (residues 147–149) and the helical region interacts with the protein, while the C-terminus does not interact with the protein and remains disordered in the ensemble of the solution structures (Fig. 3). Specifically, the helical portion of the peptide (residues 152–157) sits between the A/B helical interface, contacting the methyl group of residues A22, A23, and I26 in the A-helix and L41, K43, M47, and L48 in the B-helix. The N-terminus of the peptide extends into the hydrophobic pocket of cNTnC, making contacts to the methyl groups of M60, V82, and M85 in cNTnC. As discussed above, the N-terminal residue R147 of the peptide moves away from the tail of W7 because of the electrostatic repulsion.

2.6. Comparison of the cNTnC•Ca^{2+}•$cTnI_{147-163}$•W7 structure with the cNTnC•Ca^{2+}•$cTnI_{147-163}$, cNTnC•Ca^{2+}•W7, and cNTnC•Ca^{2+}•$cTnI_{147-163}$•bepridil structures

The conformational change in cNTnC•Ca^{2+} that occurs upon binding $cTnI_{147-163}$, bepridil, and W7 involves the straightening of the B-helix and the BC unit moving away from the NAD unit, consisting of a "closed" to "open" structural transition. This peptide- or drug-induced structural change in cNTnC•Ca^{2+} is similar to that observed for the apo to Ca^{2+}-saturated transition in sNTnC [32]. An interesting finding from the current study is that while the cNTnC in this structure exhibits an open conformation, the A/B and C/D EF hands behave as separate units. When the NAD unit of cNTnC in cNTnC•Ca^{2+}•$cTnI_{147-163}$•W7 is superimposed onto the NAD unit of cNTnC in cNTnC•Ca^{2+}•$cTnI_{147-163}$, the B-helix moved up along with $cTnI_{147-163}$ (up 4±1 Å toward the A-helix) while the C-helix moved down (Fig. 5a). As a result, the A/B pair is more closed but the C/D pair is more open. This change is also reflected in the A/B and C/D interhelical angle changes (see Table 2). It seems that the C/D pair needs to be more open to accommodate W7 and the repulsion

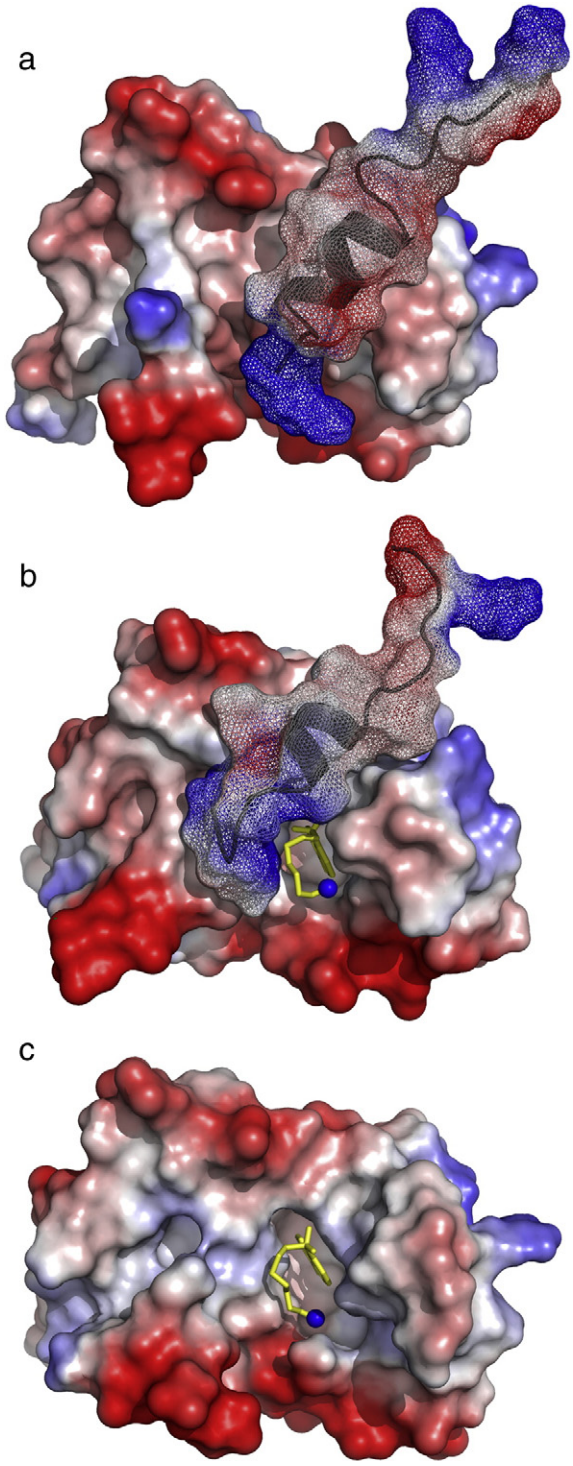

Fig. 6. Molecular surface representations of (a) cNTnC•Ca^{2+}•$cTnI_{147-163}$ (PDB, 1MXL), (b) cNTnC•Ca^{2+}•$cTnI_{147-163}$•W7 (PDB, 2KRD), and (c) cNTnC•Ca^{2+}•W7 (PDB, 2KFX). For cNTnC and $cTnI_{147-163}$, positively charged residues are shown in blue, negatively charged residues are shown in red, and other residues are shown as charge gradient. Non-hydrogen atoms of W7 are shown as stick models in yellow and nitrogen is shown in blue.

between W7 and $cTnI_{147–163}$ shifts the peptide away from the hydrophobic pocket with a concomitant destabilization of the helix. As a result, the NOE contacts between cNTnC and $cTnI_{147–163}$ from cNTnC•Ca^{2+}•$cTnI_{147–163}$ to cNTnC•Ca^{2+}•$cTnI_{147–163}$•W7 are altered. For instance, in cNTnC•Ca^{2+}•$cTnI_{147–163}$, A23 but not A22 on the A-helix makes a strong contact to L157 of $cTnI_{147–163}$ peptide, while both A22 and A23 make strong contacts to L157 in cNTnC•Ca^{2+}•$cTnI_{147–163}$•W7. When the NAD unit of cNTnC in cNTnC•Ca^{2+}•$cTnI_{147–163}$•W7 superimpose onto the NAD unit of cNTnC in cNTnC•Ca^{2+}•W7, the A/B unit did not change but the C-helix moved down (Fig. 5b, see the A/B and C/D interhelical angle changes listed in Table 2). In both the W7 bound structures, the strong NOE contacts between the hydrophobic residues in cNTnC and the naphthalene ring of W7 serve as the primary anchoring site for this molecule in the hydrophobic core of the protein. In the presence of $cTnI_{147–163}$, W7 needs to rearrange its ring and makes more contacts with the C/D interhelical interface. As a result, the C/D pair is more open. When the NAD unit of cNTnC in cNTnC•Ca^{2+}•$cTnI_{147–163}$•W7 superimpose onto the NAD unit of cNTnC in cNTnC•Ca^{2+}•$cTnI_{147–163}$•bepridil, both the A/B and C/D pairs exhibit more open interhelical angles (Fig. 5c). As a result, in cNTnC•Ca^{2+}•$cTnI_{147–163}$•W7, the BC unit is farther away from the NAD unit than that in cNTnC•Ca^{2+}•$cTnI_{147–163}$•bepridil. This could be attributed to the different effects of W7 and bepridil on the interaction of cNTnC and $cTnI_{147–163}$.

The docking of W7 and $cTnI_{147–163}$ on cNTnC is represented by comparing the molecular surfaces of cNTnC•Ca^{2+}•$cTnI_{147–163}$, cNTnC•Ca^{2+}•$cTnI_{147–163}$•W7, and cNTnC•Ca^{2+}•W7 in Fig. 6. In cNTnC•Ca^{2+}•$cTnI_{147–163}$, the helical region fit nicely between the A/B interhelical interface and the positive charged N-terminal R147 forms salt bridges with the acidic residues on the C/D helices of cNTnC (Fig. 6a). To accommodate W7, the helical region of the peptide unwinds slightly and moves up toward the A-helix while the N-terminal R147 moves away from the tail of W7 as a result of electrostatic repulsion (Fig. 6b). In the absence of $cTnI_{147–163}$, W7 finds its place in the hydrophobic pocket of cNTnC•Ca^{2+} (Fig. 6c) and it reorients its position slightly to allow the concurrent binding of $cTnI_{147–163}$ (see Fig. 5b).

In summary, the interaction between the $cTnI_{147–163}$ peptide and W7 in the cNTnC•Ca^{2+}•$cTnI_{147–163}$•W7 ternary complex makes the two ligands reorient their positions relative to those in the cNTnC•Ca^{2+}•$cTnI_{147–163}$ or cNTnC•Ca^{2+}•W7 complexes. The consequence is a rearrangement of interhelices of both AB and CD EF hands in the ternary complex than in the binary complexes. The interference between W7 and $cTnI_{147–163}$ explains the weaker affinity of $cTnI_{147–163}$ for cNTnC•Ca^{2+} in the presence of W7 than in cNTnC•Ca^{2+} alone.

2.7. Comparison of the structures of cNTnC•Ca^{2+}•$cTnI_{147–163}$•W7 and cNTnC•Ca^{2+}•W7 with the structure of CaM•$4Ca^{2+}$•2W7

The NMR structure of CaM•$4Ca^{2+}$ in complex with two W7 molecules was determined [33]. In this structure, each domain of CaM interacts with one W7 molecule. W7 binds CaM via many Van der Waals interactions between the naphthalene ring of the W7 and the hydrophobic residues of the CaM binding pocket. Osawa et al. compared the CaM binding mode between W7 and TFP and between W7 and tryptophan of CaM target peptide and concluded that the naphthalene ring is the largest that can fit into the hydrophobic pocket of CaM domain. As the N-terminal and C-terminal domains of CaM are similar, the orientation of W7 within the binding pocket is similar as well. The tail of W7 in the CaM domains is flexible but more defined in the structures of cNTnC•Ca^{2+}•W7 and cNTnC•Ca^{2+}•$cTnI_{147–163}$•W7. Thus, W7 appears to inhibit the CaM-mediated activation of target proteins by blocking the hydrophobic pocket of each domain with its naphthalene ring that normally plays a role in anchoring targets. However, in cNTnC, the tail of W7 is playing a major role in interfering with cTnC's major target, cTnI.

2.8. Relevance to the future design of cTnC-specific pharmacological agents for the treatment of heart disease

There is a need for the development of novel approaches in the therapy of heart disease. The current therapeutic paradigm for decreased systolic function is the employment of drugs that increase cytosolic Ca^{2+} levels; however, prolonged use leads to increased heart rate, hypertension, arrhythmias, and mortality. Presently, there is no drug available for the treatment of familial hypertrophic cardiomyopathy that is associated with hypertrophy and fibrosis contributing to the risk of ventricular arrhythmias and sudden cardiac death. Mutations in myofilament proteins or altered myofilament structures lead to changes in the myofilament response to Ca^{2+} and thus represent good targets for the design of novel inotropic agents. A group of Ca^{2+} sensitizers has been developed, which have been shown to increase the myocardial contractility by generating more force for a given amount of cytosolic Ca^{2+}. Levosimendan and EMD 57033 are typical examples. Recently, a new class of pharmacological agents, cardiac myosin activators (e.g., CK-1827452), has been shown to directly target the kinetics of the myosin head (for a review, see [34]). *In vitro* studies have demonstrated that these agents increase the rate of effective myosin–actin cross-bridge formation and improve myocyte energy utilization with no effect on intracellular Ca^{2+} or cAMP. Animal model and human studies have demonstrated significant increases in systolic ejection time and cardiac output, suggesting that myosin activators offer the promise of a safe and effective treatment for heart failure.

The aforementioned compounds all belong to a class of compounds known as Ca^{2+} sensitizers and are effective in treating symptoms of decreased cardiac output; however, there are less treatment options for patients suffering from impaired diastolic relaxation or increased contractility. The therapeutic advantage of compounds that target the contractile machinery was illustrated in a recent study that showed arrhythmia susceptibility caused by the Ca^{2+}-sensitizing agent EMD 57033 in animal models is prevented by the myosin inhibitor, blebbistatin [5,35]. The protective effect of blebbistatin provides the first direct evidence that Ca^{2+} desensitization in myofilaments is anti-arrhythmic and might be beneficial to individuals with hypertrophic cardiomyopathy.

The data presented in this work provide the structural basis of W7 inhibition of the regulatory cTnC–cTnI interaction. W7 functions as a Ca^{2+} desensitizer by decreasing the binding affinity of $cTnI_{147–163}$ for cNTnC•Ca^{2+}. The NMR solution structure of the cNTnC•Ca^{2+}•$cTnI_{147–163}$•W7 ternary complex furthers understanding of the molecular mechanism underlying the effects of cardiotonic drugs on the cTnC–cTnI interface. Together with a series of structures determined previously in our laboratory, it provides a molecular model important for the design of cTnC-specific cardiotonic drugs.

3. Data deposition

The atomic coordinates have been deposited in the RCSB Protein Data Bank (PDB accession code: 2KRD)

Acknowledgments

We thank Ryan Hoffman for insightful discussions. We thank David Corson and Melissa Crane for the help with the cNTnC protein expression. We would like to thank the Canadian National High Field NMR Centre (NANUC) for their assistance and use of the facilities. Operation of NANUC is funded by the Canadian Institutes of Health Research, the Natural Science and Engineering Research Council of Canada, and the University of Alberta. We would also like to acknowledge Jeff DeVries and Nicolas Shaw for spectrometer maintenance.

This work was supported by the Canadian Institutes of Health Research (Grant MOP 37760), the National Institutes of Health Grant

(R01 HL-085234), and the Heart and Stroke Foundation of Canada. Marta Oleszczuk is supported by an Alberta Heritage Foundation for Medical Research postdoctoral fellowship and Ian Robertson is supported by an Alberta Heritage Foundation for Medical Research studentship.

Appendix A. Supplementary data

Supplementary data associated with this article can be found, in the online version, at doi:10.1016/j.yjmcc.2010.01.016.

References

[1] Kobayashi T, Solaro RJ. Calcium, thin filaments, and the integrative biology of cardiac contractility. Annu Rev Physiol 2005;67:39–67.
[2] Li MX, Wang X, Sykes BD. Structural based insights into the role of troponin in cardiac muscle pathophysiology. J Muscle Res Cell Motil 2004;25:559–79.
[3] Kass DA, Solaro RJ. Mechanisms and use of calcium-sensitizing agents in the failing heart. Circulation 2006;113:305–15.
[4] Nieminen MS, Pollesello P, Vajda G, Papp Z. Effects of levosimendan on the energy balance: preclinical and clinical evidence. J Cardiovasc Pharmacol 2009;53:302–10.
[5] Baudenbacher F, et al. Myofilament Ca^{2+} sensitization causes susceptibility to cardiac arrhythmia in mice. J Clin Invest 2008;118:3893–903.
[6] Silver PJ, Pinto PB, Dachiw J. Modulation of vascular and cardiac contractile protein regulatory mechanisms by calmodulin inhibitors and related compounds. Biochem Pharmacol 1986;35:2545–51.
[7] Kleerekoper Q, Liu W, Choi D, Putkey JA. Identification of binding sites for bepridil and trifluoperazine on cardiac troponin C. J Biol Chem 1998;273:8153–60.
[8] Li Y, Love ML, Putkey JA, Cohen C. Bepridil opens the regulatory N-terminal lobe of cardiac troponin C. Proc Natl Acad Sci U S A 2000;97:5140–5.
[9] Li MX, Spyracopoulos L, Sykes BD. Binding of cardiac troponin-I147–163 induces a structural opening in human cardiac troponin-C. Biochemistry 1999;38:8289–98.
[10] Takeda S, Yamashita A, Maeda K, Maeda Y. Structure of the core domain of human cardiac troponin in the Ca(2+)-saturated form. Nature 2003;424:35–41.
[11] Wang X, Li MX, Sykes BD. Structure of the regulatory N-domain of human cardiac troponin C in complex with human cardiac troponin I147–163 and bepridil. J Biol Chem 2002;277:31124–33.
[12] Vinogradova MV, et al. Ca(2+)-regulated structural changes in troponin. Proc Natl Acad Sci U S A 2005;102:5038–43.
[13] Robertson IM, Baryshnikova OK, Li MX, Sykes BD. Defining the binding site of levosimendan and its analogues in a regulatory cardiac troponin C-troponin I complex. Biochemistry 2008;47:7485–95.
[14] Adhikari BB, Wang K. Interplay of troponin- and Myosin-based pathways of calcium activation in skeletal and cardiac muscle: the use of W7 as an inhibitor of thin filament activation. Biophys J 2004;86:359–70.
[15] Hidaka H, Yamaki T, Naka M, Tanaka T, Hayashi H, Kobayashi R. Calcium-regulated modulator protein interacting agents inhibit smooth muscle calcium-stimulated protein kinase and ATPase. Mol Pharmacol 1980;17:66–72.
[16] Li MX, Hoffman RM, Sykes BD. Interaction of cardiac troponin C with calmodulin antagonist [corrected] W7 in the presence of three functional regions of cardiac troponin I. Biochemistry 2006;45:9833–40.
[17] Hoffman RM, Li MX, Sykes BD. The binding of W7, an inhibitor of striated muscle contraction, to cardiac troponin C. Biochemistry 2005;44:15750–9.
[18] Hoffman RM, Sykes BD. Structure of the inhibitor W7 bound to the regulatory domain of cardiac troponin C. Biochemistry 2009;48:5541–52.
[19] Gemmecker G, Olejniczak ET, Fesik SW. An improved method for selectively observing protons attached to C-12 in the presence of H-1–C-13 spin pairs. J Magn Reson 1992;96:199–204.
[20] Ikura M, Bax A. Isotope-filtered 2D NMR of a protein peptide complex—study of a skeletal muscle myosin light chain kinase fragment bound to calmodulin. J Am Chem Soc 1992;114:2433–40.
[21] Ogura K, Terasawa H, Inagaki F. An Improved double-tuned and isotope-filtered pulse scheme based on a pulse field gradient and a wide-band inversion shaped pulse. J Biomol NMR 1996;8:492–8.
[22] Lee W, Revington MJ, Arrowsmith C, Kay LE. A pulsed field gradient isotope-filtered 3D ^{13}C HMQC-NOESY experiment for extracting intermolecular NOE contacts in molecular complexes. FEBS Lett 1994;350:87–90.
[23] I.M. Roberston, L. Spyracopoulos, B.D. Sykes. The evaluation of isotope editing and filtering for protein–ligand interaction elucidation by NMR. NATO Science for Peace and Security Series—B: Physics and Biophysics 2009;Biophysics and the Challenges of Emerging Threats:101-119.
[24] Delaglio F, Grzesiek S, Vuister GW, Zhu G, Pfeifer J, Bax A. NMRPipe: a multidimensional spectral processing system based on UNIX pipes. J Biomol NMR 1995;6:277–93.
[25] Johnson BA. Using NMRView to visualize and analyze the NMR spectra of macromolecules. Methods Mol Biol 2004;278:313–52.
[26] Slupsky CM, Boyko RF, Booth VK, Sykes BD. Smartnotebook: a semi-automated approach to protein sequential NMR resonance assignments. J Biomol NMR 2003;27:313–21.
[27] Guntert P. Automated NMR structure calculation with CYANA. Methods Mol Biol 2004;278:353–78.
[28] Linge JP, Williams MA, Spronk CA, Bonvin AM, Nilges M. Refinement of protein structures in explicit solvent. Proteins 2003;50:496–506.
[29] Schwieters CD, Kuszewski JJ, Tjandra N, Clore GM. The Xplor-NIH NMR molecular structure determination package. J Magn Reson 2003;160:65–73.
[30] Cornilescu G, Delaglio F, Bax A. Protein backbone angle restraints from searching a database for chemical shift and sequence homology. J Biomol NMR 1999;13:289–302.
[31] Shen Y, Delaglio F, Cornilescu G, Bax A. TALOS+: a hybrid method for predicting protein backbone torsion angles from NMR chemical shifts. J Biomol NMR 2009.
[32] Gagne SM, Tsuda S, Li MX, Smillie LB, Sykes BD. Structures of the troponin C regulatory domains in the apo and calcium-saturated states. Nat Struct Biol 1995;2:784–9.
[33] Osawa M, et al. Solution structure of calmodulin–W-7 complex: the basis of diversity in molecular recognition. J Mol Biol 1998;276:165–76.
[34] Teerlink JR. A novel approach to improve cardiac performance: cardiac myosin activators. Heart Fail Rev 2009;14:289–98.
[35] Allingham JS, Smith R, Rayment I. The structural basis of blebbistatin inhibition and specificity for myosin II. Nat Struct Mol Biol 2005;12:378–9.